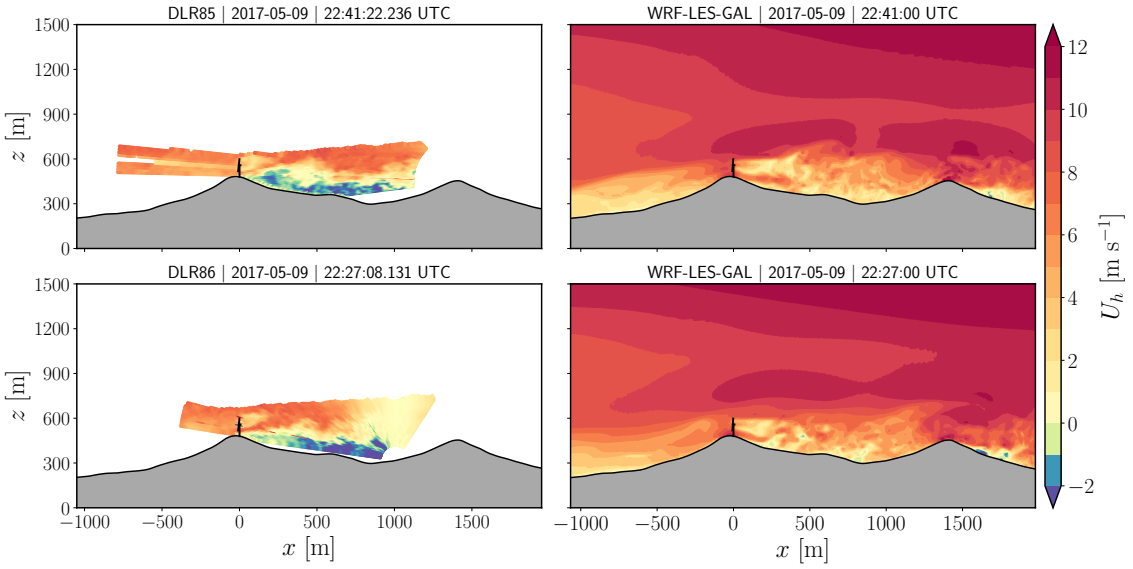


**Figure 8.19:** Comparison of instantaneous horizontal wind velocity, $U_h$, snapshots along the wake transect from the DLR85 lidar and WLGL model at approximately 22:41 (UTC) (top) and from the DLR86 lidar and WLGL model at approximately 22:27 (UTC) (bottom). The wind turbine is represented schematically by the black solid line. The results correspond to the neutral case.

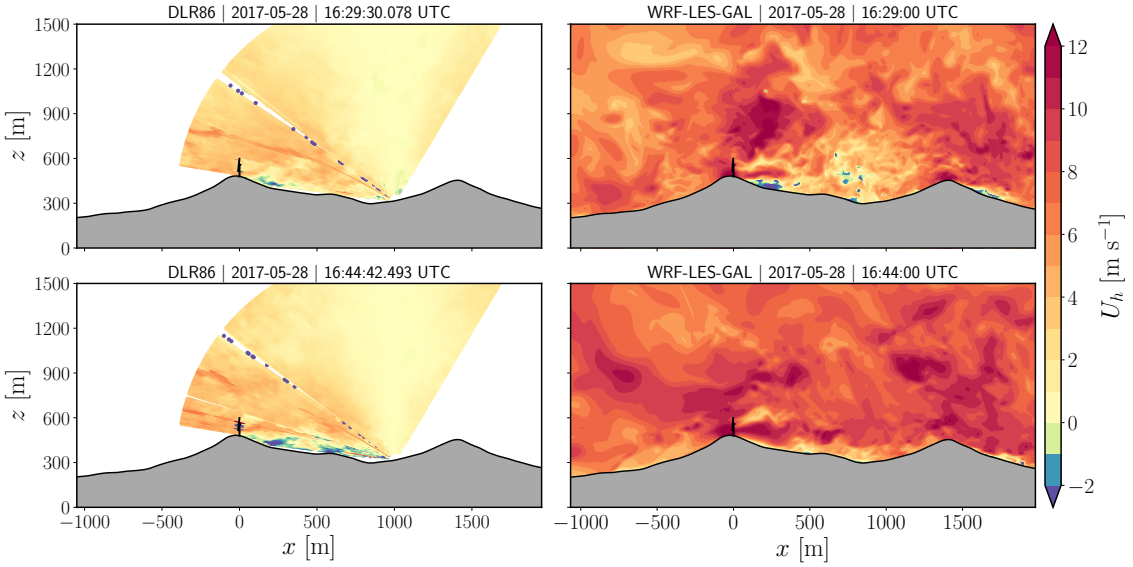


**Figure 8.20:** Comparison of instantaneous horizontal wind velocity, $U_h$, snapshots along the wake transect from the DLR86 lidar and WLGL model at approximately 16:29 (UTC) (top) and 16:44 (UTC) (bottom). The wind turbine is represented schematically by the black solid line. The results correspond to the unstable case.

underestimated in the WLGL model, compared to the mean wind velocity field captured by the DLR86 lidar. Also, while the modeled wake extends into the valley up to $\sim 2D$, a shorter wake extending up to $\sim 1D$ downstream of the wind turbine was observed in the DLR86 lidar scan.

Figure 8.24 shows 1-hour averaged horizontal wind velocity, $\overline{U}_h$, field from the DLR and

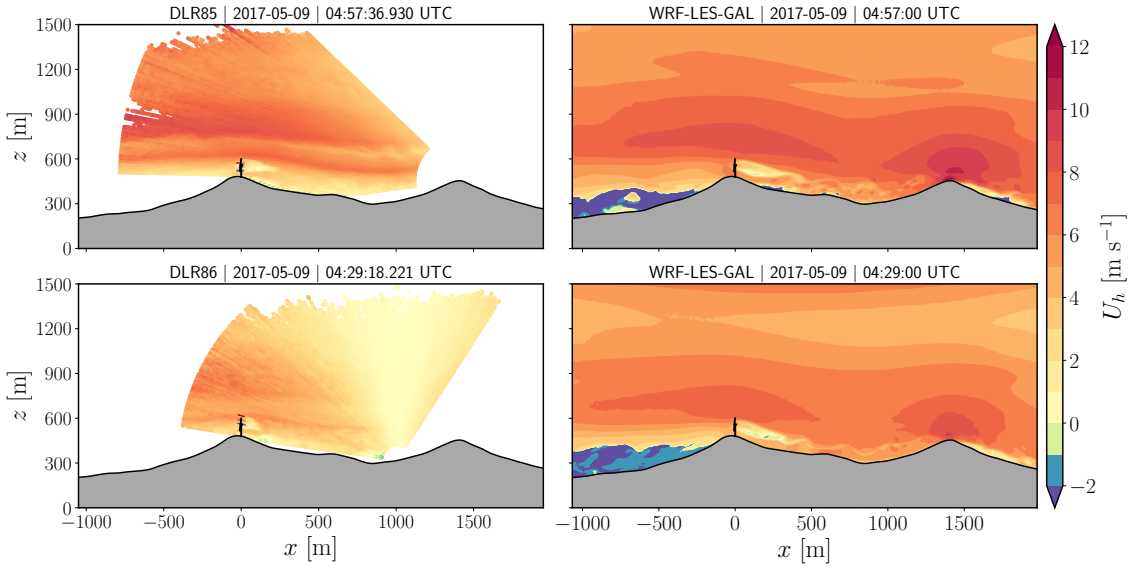


**Figure 8.21:** Comparison of instantaneous horizontal wind velocity, $U_h$, snapshots along the wake transect from the DLR86 lidar and WLGL model at approximately 16:29 (UTC) (top) and 16:44 (UTC) (bottom). The wind turbine is represented schematically by the black solid line. The results correspond to the stable case.

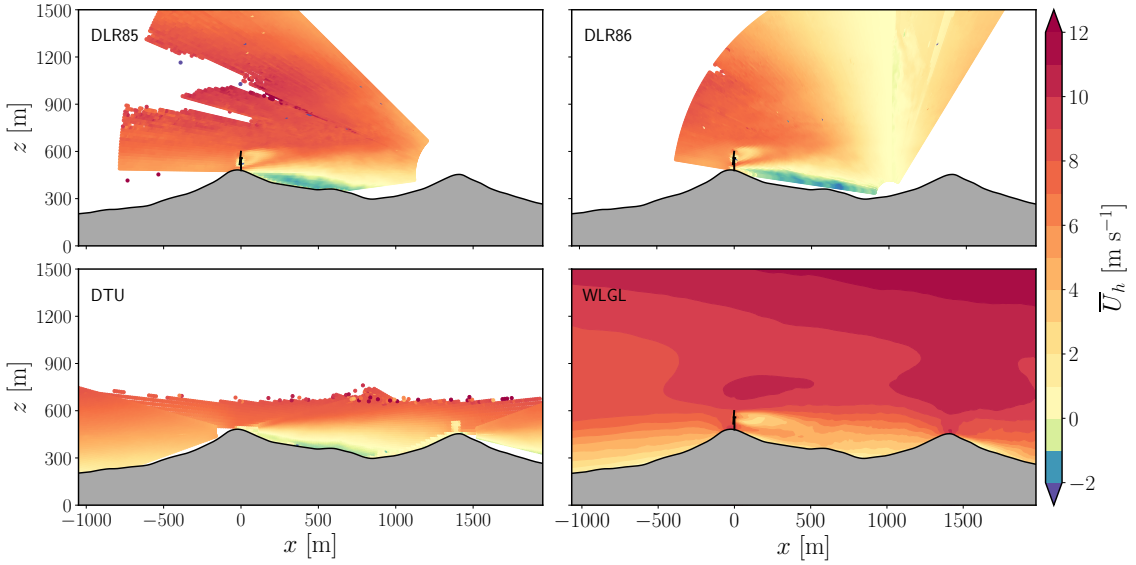


**Figure 8.22:** Comparison of 1-hour average horizontal wind velocity, $\overline{U}_h$, from the DLR85 (top left), DLR86 (top right), DTU (bottom left) lidars and WLGL model (bottom right). Note that the color map of DTU lidars is plotted along the offset transect, whereas others are cross-sections along the wake transect (see Figure 8.5 for details). The wind turbine is represented schematically by the solid black line. The results correspond to the neutral case.

DTU lidars, and WLGL model for the stable case. The average Froude number at the first ridge during the WLGL simulation of stable ABL conditions is calculated to be 1.3, resulting in a large portion of air flowing over the top of the hill, with longer mountain waves [326]. The natural wavelength of flow waves, $\lambda_w = 1325.4$ m, is much longer than the width of the first ridge, $L_h = 231.2$ m, causing the airflow to move over the mountain